**Title**

# Contribution of decomposing plant roots to $N_2O$ emissions by water absorption

By

Kyungmin Kim*, Andrey Guber, Mark Rivers, and Alexandra Kravchenko

Department of Plant Soil and Microbial Sciences, Michigan State University,

East Lansing, MI 48823, USA

Electronically Submitted to:

*Geoderma* through Elsevier Editorial System

8/11/2020

*To whom correspondence should be addressed;

Phone: 626-679-8599

Email: kimkyu46@msu.edu

**Abstract**

The "sponge effect", or water absorption by incorporated plant leaf residues, was recently identified as one of the mechanisms that drives activity in microbial hotspots. We explored the presence of the sponge effect in plant root residues, and its role in root decomposition and associated $N_2O$ and $CO_2$ emissions. Young soybean (*Glycine max*) plants were grown in microcosms with two soil materials dominated by (i) large (>30 μm Ø) and (ii) small (<10 μm Ø) pores. After termination, the microcosms with the decomposing roots were incubated at 50% and 75% water-filled pore space (WFPS) soil moisture levels. Root decomposition, water absorption by the decomposing roots, and water redistribution were quantified using X-ray computed micro-tomography, including dual-energy scanning. The results demonstrated occurrence of the sponge effect in young, *in-situ* grown soybean roots and sharp gradients in the distribution of the added liquid within ~150 μm distance from the decomposing roots. At 50% WFPS the large pore soil emitted 185% more $N_2O$ than the small pore soil; and, during the first 5 days of incubation, more $N_2O$ than the large pore soil at 75% WFPS. This finding indicates that the decomposing roots acted as hotspots of $N_2O$ production, potentially due to sponge effect and associated anoxic conditions. Our study suggests that the interactions between pore characteristics and soil moisture can play a significant role in defining the contribution of detritusphere, specifically, decomposing young roots, to soil biogeochemical processes, including microbial activity and denitrification dynamics.

## 1. INTRODUCTION

While residue incorporation brings multiple benefits to soil fertility and sustainability (Lehtinen et al., 2014), crop residues can also stimulate the emission of greenhouse gases (GHGs) from the soil (Baggs et al., 2000; Jin et al., 2014 ; Köbke et al., 2018). Roots account for 13 – 67 % of the whole plant biomass (Roy et al., 2001; Bolinder et al., 2002), thus mass of root residues remaining in the soil after the harvest can be substantial, reaching 0.5–2 $Mg \cdot ha^{-1}$ (Tufekcioglu et al., 1998).

Roots distinctly differ from aboveground biomass in terms of tissue traits and chemical composition (Kumar and Goh, 1999; Moretto et al., 2001; Kuzyakov et al., 2007; Begum et al., 2014). Such differences can cause dissimilarities in decomposition rates and C and N dynamics between the aboveground residues and roots. Lower residue quality, higher C:N ratio, and higher lignin content of root residues lead to lower C mineralization, lower denitrification, and slower decomposition compared to the leaf residues (Vanlauwe et al., 1996; Velthof et al., 2002; Bird et al., 2008; Hansson et al., 2010; Steffens et al., 2015).

Roots also differ from the incorporated aboveground residues in terms of the impact they make on the physical and chemical properties of adjacent soil. Aboveground residues are typically incorporated by mixing with tillage-disturbed soil, while roots grow, die, and decompose *in situ*, and even tillage does not fully separate decomposing roots from their associated soil. During growth, roots alter soil properties in their immediate vicinity by changing soil density, hydraulic properties, and C and N levels, as well as composition of microbial communities (Angers and Caron, 1998; Carminati and Vetterlein, 2012; Meier et al., 2017). The micro-environmental conditions created when the root was alive (i.e., rhizosphere) directly affect the conditions at which it decomposes (i.e., detritusphere).

67 The differences in compositions and in the properties of the surrounding soil can
68 potentially lead to differences in contributions of incorporated above- and belowground plant
69 residues to $CO_2$ and $N_2O$ emissions. However, the question of how much the decomposing roots
70 contribute to GHG emissions has not received as much attention as the contributions of the
71 incorporated aboveground plant residues (Hobbie et al., 2010; Chirinda et al., 2012). Moreover,
72 in most studies the roots for incubation experiments were taken from and washed of their native
73 soil before being placed into incubated microcosms (Jung et al., 2011; Bai et al., 2016; Wang et
74 al., 2017; Shahbaz et al., 2018). Thus, the potential impact on emissions from the micro-
75 environmental soil conditions created by the *in-situ* grown roots was neglected.
76 Water absorption by dry plant residue incorporated into the soil (hereafter referred to as
77 "sponge effect") affects decomposition (Iqbal et al., 2013) and has been recently identified as
78 one of the mechanisms that enhances local anoxic conditions and promotes hotspots of $N_2O$
79 emission (Kravchenko et al., 2017). Decomposition of incorporated corn and soybean leaves was
80 faster when leaves were surrounded by soil with prevalence of > 30 μm Ø pores as opposed to
81 soil dominated by ~10 μm Ø pores (Negassa et al., 2015; Kravchenko et al., 2017). Greater
82 sponge effect, i.e., higher (up to 120%) water absorption by the leaf residues, in the soil
83 dominated by the large pores was suggested as one of the drivers of faster decomposition
84 (Kravchenko et al., 2017; Kravchenko et al., 2018). Lower water retention capacity in large-pore
85 dominated soil allowed greater sponge effect compared to small-pore dominate soils. However,
86 the past work has been conducted using only aboveground plant residues. Examining the sponge
87 effect in other types of decomposing plant tissues, especially in roots, is necessary to understand

88 the role of $N_2O$ hotspots induced by plant residue decomposition in total $N_2O$ emissions from the
89 soil.

90 The objectives of this study were: i) to quantify the magnitude of the sponge effect in *in-*
91 *situ* grown roots decomposing in soils with contrasting pore size distributions and moisture
92 content levels, ii) to examine whether sponge effect changes water distribution patterns in the
93 vicinity of decomposing root residues, and iii) to quantify $N_2O$ and $CO_2$ emissions from soil with
94 decomposing root residue at contrasting soil pore size distributions and moisture content levels.
95

96 **2. MATERIALS AND METHODS**

97 *2.1 Soil microcosm preparation*

98 Soil used in the study was collected from experimental plots of the biologically based
99 agronomic treatment (corn-soybean-wheat rotation) of Long Term Ecological Research site at
100 the W.K. Kellogg Biological Station (KBS), Michigan, U.S.A. (85°24' W, 42°24' N). The soil
101 was Kalamazoo loam (fine-loamy, mixed, mesic, Typic Hapludalf), developed on glacial
102 outwash. Composite soil samples for the study were collected from 0 – 15 cm depth and air-dried.
103 The treatment design of the study consisted of two experimental factors: i) prevalent pore size,
104 with two levels, namely, soils with prevalence of > 35 μm Ø and < 10 μm Ø pores; and ii) soil
105 moisture content during the incubation, with two levels, namely, 50% and 75% WFPS.

106 To generate the two soil materials with contrasting pore sizes, we followed a method
107 described by Toosi et al. (2017). The soil material with prevalence of > 35 μm Ø pores was
108 created from 1 – 2 mm Ø fraction by sieving the air-dried soil. The soil matrial with prevalence
109 of < 10 μm Ø pores was created from the 1 – 2 mm Ø fraction by a series of gentle grindings

using mortar and pestle, followed by sieving through a 0.053 mm sieve. The remaining particles, primarily small stones, were re-collected and completely ground using a shatter box to make it pass through the 0.053 mm sieve. The use of sequential grinding to procure most of the small pore material minimized the negative effects of soil grinding on microorganisms. The two soil fractions were hereafter referred to as large-pore and small-pore soils.

Soil organic C and total N of the two materials were measured using Costech elemental combustion system (Costech Analytical Technologies, U.S.A) with 3 replicates. For inorganic N, soils were extracted using 1M KCl with soil-solution ratio of 1:5. Soil extracts were then mixed with premade reagent packets (Hach GSA, U.S.A). Salicylate method was used for ammonium and cadmium reduction method was used for nitrate (Sinsabaugh et al., 2000; Doane and Horwáth, 2003). The level of inorganic N was then determined using SYNERGY H1 (BioTek, U.S.A). Using the large soil fractions to produce the small fractions enabled us to minimize differences in soil mineralogy and microbial properties. The two soil materials were not significantly different in terms of their soil organic C, total N, $NO_3$, and $NH_4$ contents (Table. S1). The levels of the soluble organic carbon where 292 (std error 25) $\mu g\ C \cdot g^{-1}\ soil$ in the large-pore and 344 (std error 19) $\mu g\ C \cdot g^{-1}\ soil$ in the small-pore soil material and not significantly different from each other ($p$ <0.05) (reported as supplemental information by Kravchenko et al., 2017).

A total of 40 microcosms were built by packing plastic cylinders (8 mm Ø, 40 mm height) with soil of the two studied materials to a bulk density of 1.1 g $cm^{-3}$. The relatively small size of the microcosms was chosen in order to accommodate quantification of the root decomposition via X-ray μCT. A disadvantage of working with *in-situ* grown roots is the

132 unknown initial mass of roots in the system, thus the unknown loss of root mass during
133 decomposition. To quantify root decomposition during the incubation we scanned all
134 microcosms before and after the incubation (as described in section *2.4*). Then the loss of the
135 root volume was obtained as the difference in root volumes before and after the incubation μCT
136 images. While this approach enabled acceptable quantification of the root volume loss, the size
137 of the microcosms had to be kept relatively small to provide sufficiently high scanning
138 resolution.

139 On top of each microcosm cylinder we placed a larger cylinder (16 mm Ø, 5 mm height)
140 and filled it with loose soil. The purpose of the large cylinder was to accommodate the initial
141 growth of the soybean (*Glycine max*) seeds, which required more space than what was available
142 within the small cylinders. The seeds were germinated for 4-5 d on wet cloth. After germination,
143 one soybean seed was carefully inserted in the middle of each large cylinder (Fig. S1). During
144 the plant growth the soil moisture within the microcosms was initially adjusted to ~50% of
145 WFPS and 0.2 mL water was added on a daily basis to maintain optimal condition for the plant
146 growth. No fertilizers were used. The plants were allowed to grow for 4 days, the period of time
147 during which the soybeans roots grew through the entire length of the studied microcosms. Then
148 the plants were cut, and the microcosms were air-dried for 5 days.

149

150 *2.2 KI experiment*

151 Eight microcosms (2 replicates of each pore size and WFPS treatment combination) were
152 used to quantify the sponge effect and the spatial patterns in water distribution within the
153 decomposing roots. Upon root termination and air-drying, 10% potassium iodide (KI) solution
154 was added to each microcosm. Iodine is a chemical dopant that enhances the contrast of liquid

155 phase against other phases during X-ray μCT scanning (Wildenschild et al., 2002; Wildenschild
156 and Sheppard, 2013). The volume of the KI solution added to the 50% and 75% WFPS treatment
157 microcosms was equal to the respective amounts of water that were added to the counterpart
158 microcosms of these WFPS treatments in the incubation experiment (described in section 2.3).
159 The microcosms were allowed to equilibrate with added KI solution for ~24 hr and then
160 subjected to dual-energy X-ray μCT scanning (described in section 2.4).
161
162 *2.3 Incubation experiment*
163 The incubation experiment was a full factorial design with two factors: pore size with two
164 levels (prevalent large and small pores), and water content with 2 levels (50% WFPS and 75%
165 WFPS). Due to loss of 5 microcosms during handling and transporting, a total of 27 microcosms
166 (5~8 replicates of each pore size and WFPS treatment combination) were used to assess the $CO_2$
167 and $N_2O$ emissions and to quantify the root volume loss during the decomposition. To determine
168 the root volume loss the microcosms were μCT scanned twice: first, before and then, after the
169 incubation. Upon root termination and air-drying, the microcosms were subjected to X-ray μCT
170 scanning (as described in section *2.4*). Then, for the incubation, distilled water was added to the
171 tops of the microcosms to achieve the desired WFPS levels: 50% WFPS and 75% WFPS. Each
172 microcosm was placed in a 130 mL Mason jar, and a small water-filled plate was placed within
173 the jar along with the microcosm for maximizing air humidity and reducing evaporation from the
174 soil during the incubation. Completely sealed jars were incubated in the dark at 22 °C.
175 Concentrations of $CO_2$ and $N_2O$ were measured on days 1, 3, 7, 14, and 21 of the
176 incubation using Infrared Photoacoustic Spectroscopy (INNOVA Air Tech Instruments,

177 Denmark). After each gas measurement the jars were flushed with fresh air. After the incubation,
178 the microcosms were air-dried again (for 5 days) and scanned at the same µCT settings as
179 before-incubation. The µCT images obtained before and after incubation were used to calculate
180 the volume loss during the decomposition (as described in section *2.4*). Please note that even
181 though there was a 5-day time lapse between the last gas measurement and the scanning, root
182 decomposition during that period was negligible. First, the peak of active decomposition greatly
183 subsided by the end of the 21-day incubation period; second, the microcosms were placed for
184 drying into a ventilated hood and due to their small size dried very quickly (in <3 hours).
185
186 *2.4 X-ray µCT scanning and image analysis*
187 All microcosms were scanned at a resolution of 4.03 – 5.32 µm at sector 13-BM-D,
188 GeoSoilEnvironCARS, Advanced Photon Source, Argonne National Laboratory, IL. During
189 scanning two-dimensional projections were taken with 2 second exposure time and 0.25° rotation
190 angle (Quigley et al., 2018). Original projection images were reconstructed as 1200 slice images
191 with 1,920 by 1,920 pixels. Image analyses were conducted with ImageJ software (Schneider et
192 al., 2012). Before the main analysis all of the scanned images were preprocessed with Gaussian
193 blur 3D (3x3x3 window) to reduce random noise.
194 The sponge effect was assessed with the dual-energy approach (Kutlu et al., 2018), where
195 microcosms from KI experiment were scanned at two energies, 33.269 keV and 33.069 keV,
196 which are above and below the K-shell edge for iodine (33.169 keV). The mass attenuation
197 coefficients of soil particles, air and water do not change considerably when switching from one
198 energy level to another, however they do change for iodine. Therefore, subtracting the below K-

edge images from those obtained at the energy above the K-edge provides a map of iodine distribution within the microcosm (Kutlu et al., 2018; Deboodt et al., 2019), which informs of the distribution patterns of water in the soil of the studied pore size and WFPS treatments. Difference images (33.269 keV - 33.069 keV) were converted into binary images reflecting presence and absence of iodine. Threshold value for iodine was determined according to the volume ratio of KI and total soil sample. The iodine content in each medium (roots and soils) was calculated as the number of medium's voxels occupied by the iodine divided by the total number of the medium's voxels, and was expressed as percent.

The thresholds for root and soil segmentation were computed using the minimum error thresholding approach (Kittler and Illingworth, 1986). The peaks corresponding to pore space and soil mineral material were clearly visible on the histograms of images (Fig. S2). Two Gaussian distributions, for pore and soil mineral, were fitted to histograms of grayscale images (Nakagawa and Rosenfeld, 1979; Kravchenko et al., 2019). The grayscale value corresponding to the pore peak, i.e., pore mean, plus two standard deviations was used as the lower boundary for root identification. The grayscale value corresponding to the mineral peak, i.e., mineral mean, minus two standard deviations was used as the upper boundary for root identification. After the initial root thresholding using the lower and upper boundaries, surfaces of identified roots were manually cleaned to increase the accuracy of root separation, followed by a series of filling holes, erosion, and dilation (1 iteration) operations using 3D erode and dilate tools of BoneJ. That helped with removing the partial volume effects and cleaning the surface of the root residue. Final removal of the remaining artifacts was achieved using particle identification tool of BoneJ, ‘Particle Analyzer’, with the options of minimum value as 6; maximum value as infinite; surface resampling and volume resampling as 2; and gradient split as 0.

From the dual-energy scanned images, we assessed the iodine contents as a function of the distance from the roots. For that we used 3D dilation tools from BoneJ plugin of ImageJ (Doube et al., 2010) to create 7 layers around each root. The layers followed the shape of the root and covered distances 0-48, 48-96, 96-144, 144-192, 192-240, 240-480, and 480-720 μm from the surface of the root (Fig. S3). Only the soil mineral voxels from the layers were used in iodine calculations, while all pore voxels were excluded. The iodine contents in each layer was calculated as the percent of the voxels occupied by iodine divided by the total number of soil mineral voxels within the layer.

The microcosms from the incubation experiment were scanned at 28 keV energy both before- and after-incubation. Root binary images of before- and after-incubation were obtained, and the decomposition of the root was expressed as the root volume loss (%).

$$Volume\ loss = (1 - \frac{V_a}{V_b}) \times 100 \qquad (1)$$

where, $V_a$ and $V_b$ are the numbers of root voxels in the image sequences scanned after- and before- incubation, respectively.

*2.5 Statistical analysis*

The statistical models used in the data analyses varied for different response variables depending on the specific experimental design settings. The root volume loss data originated from a completely randomized design and were analyzed using the statistical model with fixed factor i.e., pore size and WFPS, and their interaction. The iodine content in the two media, i.e., soil vs. root, within each microcosm was analyzed using the statistical model with the fixed effects of pore size, WFPS, medium type, their interactions, and a random effect of the

244 microcosm nested within pore size and WFPS, which was used as an error term to test the effect
245 of the pore size and WFPS. The data on iodine content as a function of the distance from the root
246 were analyzed using the statistical model with the fixed effects of pore size, WFPS, layer, and
247 their interactions. Microcosm was included as a random effect and used as an error term to test
248 the effect of the pore size and WFPS. The $CO_2$ and $N_2O$ fluxes were analyzed using a repeated
249 measures approach as described in Milliken and Johnson (2009). For that, the statistical model
250 consisted of fixed effects of pore size, WFPS, incubation time, and their interactions. The model
251 also included a random effect of the microcosms nested within pore size and WFPS, which was
252 used as an error term to test their effects and as a subject for repeated measurements. Model
253 selection was conducted using Akaike Information Criterion and Bayesian Information Criterion.
254 All analyses were conducted in PROC MIXED of SAS 9.4 (SAS Inc, 2017). Summary of the F-
255 tests for the studied statistical models are shown in Supplementary Tables S2 – S8.
256 In all analyses the normality assumption was checked using normal probability plots of
257 the residuals. The equal variance assumption was evaluated by examining the plots of the
258 predicted versus residual values and the side-by-side box plots of the residuals (Fernandez, 1992;
259 Kuehl, 2000; Ott and Longnecker, 2015). When the assumptions were found to be violated, the
260 data were subjected to natural log-transformation. Reported are log-transformed values, but
261 back-transformed means and 95% confidence intervals are provided in Table S9.
262 Slicing, a.k.a. simple effect test of the interactions, was performed for all pre-planned
263 interaction comparisons. The differences between the treatment means were reported as
264 statistically significant based on the slicing results. The results are reported as statistically
265 significant at $p < 0.05$ and as trends and tendencies at $p < 0.10$ levels. The figures were produced

using Python version 3.6 (Python Software Foundation, https://www.python.org/). Error bars in all figures indicate standard errors.

## 3. RESULTS

### *3.1 Sponge effect in decomposing roots assessed through iodine distribution patterns*

Roots held significantly higher amounts of added iodine than surrounding soil in all WFPS and pore size groups ($p < 0.05$, Fig. 1 and Table S2). At 50% WFPS, the root volumes with iodine in the large-pore microcosms were 9.4 % greater than that in the roots in the small-pore microcosms ($p < 0.05$, Table S3). However, the root volume with iodine at 75% WFPS was not significantly different between the pore size groups.

Iodine content in the soil immediately adjacent to the roots (~ 48 μm) was noticeably higher than in the bulk soil matrix (> 720 μm from roots; $p < 0.05$). In all treatments, iodine content decreased markedly at 0-96 μm distance from the roots and reached its background level (i.e., iodine content in the bulk soil matrix) ~150 μm from the roots (Fig. 2). While there was no significant difference between pore sizes at 75% WFPS, large-pore microcosms had greater iodine content in the soil at 0-48 μm distance from the roots, compared to small-pore soils at 50% WFPS ($p < 0.05$, Fig. 2 and Table S5). That is, the gradient created at 0-96 μm distance from the roots in large-pore soil was higher than the one created in small-pore soil.

### *3.2. Root decomposition*

The loss of root volume was higher in the microcosms of the large- than the small-pore size group at 50% WFPS ($p < 0.05$, Fig. 3 and Table S7). In the small-pore microcosms, 75%

288 WFPS tended to lead to a greater root volume loss compared to that in 50% WFPS ($p < 0.10$,
289 Table S7).
290
291 *3.3 $CO_2$ and $N_2O$ emissions during the incubation*
292 The large-pore microcosms had higher $CO_2$ emission rates compared to the small-pore
293 microcosms on days 3, 14, and 21 of the incubation at 50% WFPS (Fig. 4a). However, there was
294 no significant difference in $CO_2$ emissions between the two pore sizes at 75% WFPS (Fig. 4b).
295 WFPS had no effect on the cumulative amounts of emitted $CO_2$.
296 At 50% WFPS, $N_2O$ emission in the large-pore microcosms was significantly higher than
297 that in the small-pore microcosms throughout the incubation period (Fig. 4c). In contrast, at 75%
298 WFPS, $N_2O$ emission tended to be higher in the small- than in the large-pore microcosms (Fig.
299 4d). The difference was especially pronounced during the first 3 days of the incubation and
300 disappeared afterwards. Cumulative $N_2O$ emission exhibited a similar pattern; at 50% WFPS
301 emission from the large-pore microcosms exceeded that from the small-pore microcosms, while
302 at 75% WFPS small-pore emissions exceeded the large-pore ones (Fig. S4).
303 The effect of WFPS on $N_2O$ emissions from the large- and small-pore microcosms
304 depended on the incubation time (Fig. 5). In the small-pore microcosms greater $N_2O$ emissions at
305 75% than at 50% WFPS were observed from the start of the incubation and continued for the
306 entire incubation period (Fig. 5b). In the large-pore microcosms, greater $N_2O$ emissions at 75%
307 than at 50% WFPS were also observed for a substantial period of time during the incubation, but
308 only starting from day 5-6. However, during the first ~5 days, greater emissions took place at
309 50% than at 75% WFPS (Fig. 5a). In the small-pore microcosms cumulative $N_2O$ emission was
310 greater at 75% than at 50% WFPS ($p < 0.05$), while WFPS effect was not statistically significant

311 in the large-pore microcosms (Fig. S4). F-value and *p*-value for the treatment effects are
312 provided in Table S8.

313 Additional information on $N_2O$ emissions from bare soil microcosms (i.e., without root
314 residue) under 50% WFPS was presented in Fig. S5. Initial $N_2O$ emission from bare soils were
315 much lower (< 0.2 μg $N_2O$-N $kg^{-1}$·soil·$day^{-1}$) compared to the microcosms with root residues (>
316 10 μg $N_2O$-N $kg^{-1}$·soil·$day^{-1}$). There was a significant difference in $N_2O$ emission between large-
317 pore bare soils and small-pore bare soils only at day 3 of the incubation ($p < 0.05$).
318
319 **4. DISCUSSION**
320 *4.1 Water absorption by decomposing plant roots – the sponge effect*
321 The KI solution was preferentially absorbed by the decomposing plant roots, with a
322 minor amount remaining in the soil itself (Fig. 1). This indicates the presence of the sponge
323 effect in root residue, which is consistent with previously reported findings of the sponge effect
324 in leaf and stem residues of different plant species (Iqbal et al., 2013; Kravchenko et al., 2017).
325 While the transformation of iodide into organoiodine upon contact with organic material likely
326 also took place (Yamaguchi et al., 2010), the redistribution of the liquid added into the air-dry
327 microcosms by the capillary forces can be regarded as the main driving force for the resultant
328 iodine attenuation patterns.
329 Greater sponge effect in the large-pore soil at 50% WFPS (Fig. 1b and 1d) resulted from
330 the lower water retention capacity of large pores, thus greater matric potential gradient between
331 decomposing plant residue and surrounding soil (Kutlu et al., 2018). However, at 75% WFPS,
332 roots in both large- and small-pore soils had similarly high iodine contents, close to their full

saturation (Fig. 1c). Kutlu et al. (2018) demonstrated that while the water content of the soybean leaves was greater in the large-pore microcosms rather than in the small-, when soil moisture content ranged from 18–36 % WFPS, the difference disappeared as soil moisture content exceeded 73% WFPS. Consistent with our findings, as water content increased (75% WFPS) the differences in iodine contents between the pore size treatments disappeared.

Water distribution gradient from the decomposing roots into soil matrix (Fig. 2) reflected the liquid levels within the roots themselves (Fig. 1) and were the strongest in 75% WFPS samples, followed by 50% WFPS large pore samples and then the 50% small pore samples. This suggests that the overall gradient in water and iodine levels between the roots and the soil matrix was the main driving force behind the observed trends.

While micro-scale patterns in water distribution in the rhizosphere have been assessed before (Carminati et al., 2010), to our knowledge, this is the first time that the water gradients next to decomposing roots were evaluated on a μm scale. Further studies of the micro-scale patterns in water re-distribution within detritusphere are needed, since such patterns can influence microscale redox conditions, microbial activity (e.g., aerobic, anaerobic) hotspots, and thus heterogeneous C and N turnover rates.

*4.2 Root decomposition and $CO_2$ emission*

Greater root decomposition in large-pore soil at 50% WFPS as compared to the small-pore soil (Fig. 3b) is consistent with previously reported aboveground residue decomposition findings. Greater corn leaf volume loss was observed in the large- (> 30 μm) than in the small- (< 10 μm) pore soil at 35 ~ 50% WFPS (Negassa et al., 2015; Kravchenko et al., 2017), and

355 greater wheat residue decomposition was associated with 15-60 μm than < 4 μm pores (Strong et
356 al., 2004). Coppens et al. (2007) showed that maximized water content of the plant residue can
357 increase the decomposition rate by PASTIS (Prediction of Agricultural Solute Transport In Soil)
358 model scenario analysis.

359 Cumulative $CO_2$ emissions were not affected by soil WFPS. Consistent with this
360 observation, negligible response of $CO_2$ emission to the soil moisture was reported by Ruser et
361 al. (2006) at 40 - 90% WFPS and by Moyano et al. (2012) at > 40% WFPS. Since the soil WFPS
362 in this study was within an optimal range for microbes, WFPS was probably not a limiting factor
363 for microbial respiration. The influence of pore size on $CO_2$ emissions depended on the soil
364 moisture content. At 50% WFPS, we observed greater $CO_2$ emission from the large- rather than
365 the small-pore microcosms (Fig. 4a), consistent with the higher root volume losses. While, no
366 differences between the pore-size treatments were observed at 75% WFPS.

367 The observed higher $CO_2$ emissions from large rather than from small-pore treatments at
368 50% WFPS contradict other decomposition experiments with soil of contrasting particle sizes,
369 where greater $CO_2$ emissions typically occurred in finer soil materials (Rastogi et al., 2002;
370 Oertel et al., 2016). Greater $CO_2$ emission in the small pore dominated soil was also reported in
371 the studies conducted previously in our research group (Negassa et al., 2015; Toosi et al., 2017).
372 This discrepancy is likely brought by the differences in timings between soil material
373 preparations and incubation experiments. In the process of grinding the large aggregate fraction
374 to procure the small-pore material, the organic carbon originally protected within large
375 aggregates typically becomes available for decomposition (Balesdent et al., 2000). Available C
376 in crushed soil causes a burst of $CO_2$ when it is wetted (Van Veen and Kuikman, 1990; Jarvis et
377 al., 2007). Other studies (e.g., Negassa et al., 2015; Toosi et al., 2017) monitored $CO_2$ emission

immediately after wetting, capturing the burst of $CO_2$ in freshly ground soil. Meanwhile, the burst of $CO_2$ was not captured in this study because soil was wetted several days before the incubation, i.e., at planting, and was kept in moist and wet conditions during the 4 days of plant growth.

*4.3 $N_2O$ emission*

It should be noted that the two studied soil materials did not differ substantially in terms of either total C and N, and/or inorganic N contents (Table S1). $N_2O$ emissions from the control soil were very low in both materials, and, as expected, tended to be somewhat higher in the small pore than in the large pore treatment (Fig. S5), due to greater anaerobic conditions within the former. Presence of decomposing roots increased $N_2O$ emission ten to hundred-fold compared to the controls and markedly changed the pattern of differences in $N_2O$ emissions between large and small pore materials (Fig. 4). These results add to the growing evidence of the importance of interactions among pore architecture, soil moisture, and plant residues for soil biogeochemical processes, including microbial oxygen consumption and denitrification dynamics (Ebrahimi and Or, 2018; Schlüter et al., 2018).

The presence of root residue changed the temporal dynamic of soil moisture influence on $N_2O$ emissions. After the first 5 days of incubation, the $N_2O$ emissions were higher at 75% than at 50% WFPS in both large and small-pore soil microcosms (Fig. 5). This result is consistent with a large body of previous work reporting that $N_2O$ emission increases along the soil moisture content gradient, reaching maximum at 75% - 100% WFPS (e.g., Khalil and Baggs, 2005; Ciarlo et al., 2007). Denitrification is the main source of $N_2O$ production in the anoxic soil matrix at

400 such high moisture levels (Groffman and Tiedje, 1989; McTaggart et al., 2002; Ciarlo et al.,
401 2007; van der Weerden et al., 2012).

402 However, during the first 5 days of incubation, an opposite trend was observed in the
403 large-pore microcosms: $N_2O$ emission was significantly higher at 50% than at 75% WFPS. This
404 result can be attributed to the influence of the decomposing roots. At the start of the incubations
405 (first ~ 5 days), at 50% WFPS, higher amounts of water were absorbed by the root residues in the
406 large-pore than in the small-pore microcosms (Fig. 2a). The high moisture levels within the
407 residues enhanced root decomposition (Fig. 3b), likely providing greater amounts of available C
408 (Gaillard et al., 1999; Gaillard et al., 2003), and turned the root into a local hotspot of anoxic
409 conditions (Li et al., 2016). The large amounts of $N_2O$ produced within the decomposing roots
410 during the first 5 days of incubation then quickly escaped via atmosphere connected pores
411 dominating the large pore microcosms. Later into the incubation (> 5 days) the contribution of
412 the roots to $N_2O$ production decreased, and the emitted $N_2O$ was probably dominated by the
413 production from within the soil matrix itself. Subsequently, the $N_2O$ emissions became higher in
414 the microcosms with higher (75% WFPS) bulk soil moisture level.

415 In the small-pore microcosms at 50% WFPS, the contribution of roots to the initial $N_2O$
416 production and emission was probably lower than in the large-pore microcosms. That could be
417 caused by slower root decomposition (Fig. 3b and 4a) limiting the sources of C/N required for
418 microbes to produce $N_2O$ and weaker sponge effect in the root forming less extreme anoxic
419 conditions within the root (Fig. 1b). Therefore, in the small-pore soil, WFPS was the main
420 driving force of the $N_2O$ emissions during the entire incubation period.

421 Our findings suggest that in soil with a dominance of > 30 µm pores, the contribution of
422 decomposing roots to $N_2O$ emission can be substantial and, as a result, the bulk soil WFPS

423 characteristics might not be a reliable $N_2O$ emission predictor (Li et al., 2016). These
424 observations concur with results from several other studies. For example, Velthof et al. (2002)
425 reported greater total $N_2O$ emission from Brussels sprouts, mustard, and broccoli residues in
426 sandy compared to clay soil. Weak associations between bulk soil moisture content and $N_2O$
427 emissions in residue amended soil is another supporting example: during decomposition of *Vicia*
428 *villosia*, no correlation between moisture level and $N_2O$ emission was observed at the beginning
429 of incubation (Shelton et al., 2000). Also, $N_2O$ emission was not proportional to soil moisture
430 content (40% - 60% WFPS) in the soil where *Trifolium pratense L.* and *Vicia villosa* were
431 incorporated (Li et al., 2016).
432 It should be noted that a formal quantification of the contribution of decomposing roots to
433 the overall amounts of emitted $N_2O$ was not conducted in this study. Such quantification will be
434 needed to fully assess the potential contribution of decomposing roots to hotspot $N_2O$ production
435 and will be the subject of further investigation. Also, young legume roots used in this study tend
436 to have low C:N ratios, likely resulting in maximal $N_2O$ productions and emissions (Velthof et
437 al., 2002; Huang et al., 2004). While, quantitatively, our findings may not fully represent the
438 effects from decomposing older roots in the field, they do provide insights on the factors
439 contributing to hot-spot $N_2O$ production and emissions from *in-situ* grown roots.
440
441 **4. Summary and conclusions**
442 The study demonstrated that the sponge effect was present in young decomposing
443 soybean roots. Up to 62.6 % greater amounts of the added liquid accumulated within the roots
444 than within the soil. The added liquid formed a distribution gradient around the roots, decreasing
445 with increasing distance from the roots until reaching background soil levels at a distance of

~150 µm. To our best knowledge, this is the first time when the water gradients next to decomposing roots were evaluated on an µm scale using X-ray µCT image analysis. Further studies of the micro-scale patterns in water re-distribution within detritusphere are needed, since such patterns can influence microscale redox conditions, microbial activity (e.g., aerobic, anaerobic) hotspots, and thus heterogeneous C and N turnover rates.

At medium soil moisture (50% WFPS) the large-pore dominated soil emitted greater amounts of $N_2O$ than the small pore soil, and, surprisingly, even more $N_2O$ than the large pore soil at high soil moisture (75% WFPS). This finding suggests that the decomposing root residues acted as hot spots of $N_2O$ production, probably due to enhanced sponge effect and associated local anoxic conditions. However, after approximately 5 days of incubation the $N_2O$ emission at 50% WFPS became lower than that at 75% WFPS, indicating that the contribution of the decomposing roots to $N_2O$ production declined. At high soil moisture (75% WFPS) and in the absence of roots, greater $N_2O$ emissions were observed from the soil dominated by small pores.

**Acknowledgements**

This work was funded in part by the National Science Foundation's Geobiology and Low Temperature Geochemistry Program (Award number 1630399). This material is based upon work supported in part by the Great Lakes Bioenergy Research Center, U.S. Department of Energy, Office of Science, Office of Biological and Environmental Research under Award Number DE-SC0018409. This research used resources of the Advanced Photon Source, a U.S. Department of Energy (DOE) Office of Science User Facility operated for the DOE Office of Science by Argonne National Laboratory under Contract No. DE-AC02-06CH11357. We appreciate the support from Michigan State University Environmental Science and Policy

469 Program (ESPP). Also, we thank Michelle Quigley and Maxwell Oerther for help with
470 laboratory analysis.

471 **5. REFERENCE**

472 Angers, D.A., Caron, J., 1998. Plant-induced changes in soil structure: processes and
473 feedbacks. Biogeochemistry 42, 55-72.

474 Bai, Z., Liang, C., Bodé, S., Huygens, D., Boeckx, P., 2016. Phospholipid 13C stable
475 isotopic probing during decomposition of wheat residues. Applied Soil Ecology 98, 65-74.

476 Baggs, E., Rees, R., Smith, K., Vinten, A., 2000. Nitrous oxide emission from soils after
477 incorporating crop residues. Soil use and management 16, 82-87.

478 Bateman, E., Baggs, E., 2005. Contributions of nitrification and denitrification to N 2 O
479 emissions from soils at different water-filled pore space. Biology and fertility of soils 41, 379-
480 388.

481 Groffman, P.M., Tiedje, J.M., 1989. Denitrification in north temperate forest soils: spatial and
482 temporal patterns at the landscape and seasonal scales. Soil Biology and Biochemistry 21, 613-
483 620.

484 Begum, N., Guppy, C., Herridge, D., Schwenke, G., 2014. Influence of source and quality
485 of plant residues on emissions of N 2 O and CO 2 from a fertile, acidic Black Vertisol. Biology
486 and fertility of soils 50, 499-506.

487 Bird, J.A., Kleber, M., Torn, M.S., 2008. 13C and 15N stabilization dynamics in soil
488 organic matter fractions during needle and fine root decomposition. Organic Geochemistry 39,
489 465-477.

490 Bolinder, M., Angers, D., Bélanger, G., Michaud, R., Laverdière, M., 2002. Root biomass
491 and shoot to root ratios of perennial forage crops in eastern Canada. Canadian Journal of Plant
492 Science 82, 731-737.
493 Carminati, A., Moradi, A.B., Vetterlein, D., Vontobel, P., Lehmann, E., Weller, U., Vogel,
494 H.-J., Oswald, S.E., 2010. Dynamics of soil water content in the rhizosphere. Plant and Soil 332,
495 163-176.
496 Carminati, A., Vetterlein, D., 2012. Plasticity of rhizosphere hydraulic properties as a key
497 for efficient utilization of scarce resources. Annals of botany 112, 277-290.
498 Chen, H., Li, X., Hu, F., Shi, W., 2013. Soil nitrous oxide emissions following crop residue
499 addition: a meta-analysis. Global change biology 19, 2956-2964.
500 Chirinda, N., Olesen, J.E., Porter, J.R., 2012. Root carbon input in organic and inorganic
501 fertilizer-based systems. Plant and Soil 359, 321-333
502 Ciarlo, E., Conti, M., Bartoloni, N., Rubio, G., 2007. The effect of moisture on nitrous
503 oxide emissions from soil and the N 2 O/(N 2 O+ N 2) ratio under laboratory conditions. Biology
504 and fertility of soils 43, 675-681.
505 Coppens, F., Garnier, P., Findeling, A., Merckx, R., Recous, S., 2007. Decomposition of
506 mulched versus incorporated crop residues: modelling with PASTIS clarifies interactions
507 between residue quality and location. Soil Biology and Biochemistry 39, 2339-2350.
508 Deboodt, T., Wildenschild, D., Ideker, J.H., Isgor, O.B., 2019. Use of iodide for improving
509 phase quantification using x-ray tomography. Cement and Concrete Research 116, 102-112.
510 Doane, T.A., Horwáth, W.R., 2003. Spectrophotometric determination of nitrate with a
511 single reagent. Analytical letters 36, 2713-2722.

Doube, M., Kłosowski, M.M., Arganda-Carreras, I., Cordelières, F.P., Dougherty, R.P., Jackson, J.S., Schmid, B., Hutchinson, J.R., Shefelbine, S.J., 2010. BoneJ: free and extensible bone image analysis in ImageJ. Bone 47, 1076-1079.

Ebrahimi, A., Or, D., 2018. Dynamics of soil biogeochemical gas emissions shaped by remolded aggregate sizes and carbon configurations under hydration cycles. Global change biology 24, e378-e392.

Fernandez, G.C., 1992. Residual analysis and data transformations: important tools in statistical analysis. HortScience 27, 297-300.

Gaillard, V., Chenu, C., Recous, S., 2003. Carbon mineralisation in soil adjacent to plant residues of contrasting biochemical quality. Soil Biology and Biochemistry 35, 93-99.

Gaillard, V., Chenu, C., Recous, S., Richard, G., 1999. Carbon, nitrogen and microbial gradients induced by plant residues decomposing in soil. European Journal of Soil Science 50, 567-578.

Gale, W., Cambardella, C., 2000. Carbon dynamics of surface residue–and root-derived organic matter under simulated no-till. Soil Science Society of America Journal 64, 190-195.

Hansson, K., Kleja, D.B., Kalbitz, K., Larsson, H., 2010. Amounts of carbon mineralised and leached as DOC during decomposition of Norway spruce needles and fine roots. Soil Biology and Biochemistry 42, 178-185.

Hobbie, S.E., Oleksyn, J., Eissenstat, D.M., Reich, P.B., 2010. Fine root decomposition rates do not mirror those of leaf litter among temperate tree species. Oecologia 162, 505-513.

Huang, Y., Zou, J., Zheng, X., Wang, Y., Xu, X., 2004. Nitrous oxide emissions as influenced by amendment of plant residues with different C: N ratios. Soil Biology and Biochemistry 36, 973-981.

Iqbal, A., Beaugrand, J., Garnier, P., Recous, S., 2013. Tissue density determines the water storage characteristics of crop residues. Plant and Soil 367, 285-299.

Jarvis, P., Rey, A., Petsikos, C., Wingate, L., Rayment, M., Pereira, J., Banza, J., David, J., Miglietta, F., Borghetti, M., 2007. Drying and wetting of Mediterranean soils stimulates decomposition and carbon dioxide emission: the "Birch effect". Tree physiology 27, 929-940.

Jin, V.L., Baker, J.M., Johnson, J.M.-F., Karlen, D.L., Lehman, R.M., Osborne, S.L., Sauer, T.J., Stott, D.E., Varvel, G.E., Venterea, R.T., 2014. Soil greenhouse gas emissions in response to corn stover removal and tillage management across the US Corn Belt. BioEnergy Research 7, 517-527.

Jung, J.Y., Lal, R., Ussiri, D.A., 2011. Changes in CO 2, 13 C abundance, inorganic nitrogen, β-glucosidase, and oxidative enzyme activities of soil during the decomposition of switchgrass root carbon as affected by inorganic nitrogen additions. Biology and Fertility of Soils 47, 801-813.

Keiluweit, M., Wanzek, T., Kleber, M., Nico, P., Fendorf, S., 2017. Anaerobic microsites have an unaccounted role in soil carbon stabilization. Nature communications 8, 1771.

Khalil, M., Baggs, E., 2005. CH4 oxidation and N2O emissions at varied soil water-filled pore spaces and headspace CH4 concentrations. Soil Biology and Biochemistry 37, 1785-1794.

Kittler, J., Illingworth, J., 1986. Minimum error thresholding. Pattern Recognition 19, 41–47.

555 Köbke, S., Senbayram, M., Pfeiffer, B., Nacke, H., Dittert, K., 2018. Post-harvest N2O
556 and CO2 emissions related to plant residue incorporation of oilseed rape and barley straw depend
557 on soil NO3-content. Soil and Tillage Research 179, 105-113.
558 Kravchenko, A., Guber, A., Razavi, B., Koestel, J., Blagodatskaya, E., Kuzyakov, Y.,
559 2019. Spatial patterns of extracellular enzymes: Combining X-ray computed micro-tomography
560 and 2D zymography. Soil Biology and Biochemistry.
561 Kravchenko, A., Fry, J., Guber, A., 2018. Water absorption capacity of soil-incorporated
562 plant leaves can affect N2O emissions and soil inorganic N concentrations. Soil Biology and
563 Biochemistry 121, 113-119.
564 Kravchenko, A., Toosi, E., Guber, A., Ostrom, N., Yu, J., Azeem, K., Rivers, M.,
565 Robertson, G., 2017. Hotspots of soil N 2 O emission enhanced through water absorption by
566 plant residue. Nature Geoscience 10, 496.
567 Kravchenko, A.N., Negassa, W.C., Guber, A.K., Rivers, M.L., 2015. Protection of soil
568 carbon within macro-aggregates depends on intra-aggregate pore characteristics. Scientific
569 reports 5, 16261.
570 Kumar, K., Goh, K., 1999. Crop residues and management practices: effects on soil
571 quality, soil nitrogen dynamics, crop yield, and nitrogen recovery, Advances in agronomy.
572 Elsevier, pp. 197-319.
573 Kutlu, T., Guber, A.K., Rivers, M.L., Kravchenko, A.N., 2018. Moisture absorption by
574 plant residue in soil. Geoderma 316, 47-55.
575 Kuzyakov, Y., Hill, P.W., Jones, D.L., 2007. Root exudate components change litter
576 decomposition in a simulated rhizosphere depending on temperature. Plant and Soil 290, 293-
577 305.

578 Lal, R., 2005. World crop residues production and implications of its use as a biofuel.
579 Environment International 31, 575-584.
580 Lehtinen, T., Schlatter, N., Baumgarten, A., Bechini, L., Krüger, J., Grignani, C.,
581 Zavattaro, L., Costamagna, C., Spiegel, H., 2014. Effect of crop residue incorporation on soil
582 organic carbon and greenhouse gas emissions in European agricultural soils. Soil use and
583 management 30, 524-538.
584 Li, X., Sørensen, P., Olesen, J.E., Petersen, S.O., 2016. Evidence for denitrification as
585 main source of N2O emission from residue-amended soil. Soil Biology and Biochemistry 92,
586 153-160.
587 Littell, R.C., Milliken, G.A., Stroup, W.W., Wolfinger, R.D., Oliver, S., 2006. SAS for
588 Mixed Models, Second Edition. SAS Publishing.
589 McTaggart, I.P., Akiyama, H., Tsuruta, H., Ball, B.C., 2002. Influence of soil physical
590 properties, fertiliser type and moisture tension on N 2 O and NO emissions from nearly saturated
591 Japanese upland soils. Nutrient Cycling in Agroecosystems 63, 207-217.
592 Meier, I.C., Finzi, A.C., Phillips, R.P., 2017. Root exudates increase N availability by
593 stimulating microbial turnover of fast-cycling N pools. Soil Biology and Biochemistry 106, 119-
594 128.
595 Milliken, G.A., Johnson, D.E., 2009. Analysis of messy data volume 1: designed
596 experiments vol. 1. Chapman & Hall/CRC, London.
597 Moretto, A.S., Distel, R.A., Didone, N.G., 2001. Decomposition and nutrient dynamic of
598 leaf litter and roots from palatable and unpalatable grasses in a semi-arid grassland. Applied Soil
599 Ecology 18, 31-37.

Moyano, F.E., Vasilyeva, N.A., Bouckaert, L., Cook, F., Craine, J.M., Don, A., Epron, D., Formanek, P., Franzluebbers, A., Ilstedt, U., 2012. The moisture response of soil heterotrophic respiration: interaction with soil properties. Biogeosciences 9, 1173-1182.

Nakagawa, Y., Rosenfeld, A., 1979. Some experiments on variable thresholding. Pattern recognition 11, 191-204.

Negassa, W.C., Guber, A.K., Kravchenko, A.N., Marsh, T.L., Hildebrandt, B., Rivers, M.L., 2015. Properties of soil pore space regulate pathways of plant residue decomposition and community structure of associated bacteria. PLoS One 10, e0123999.

Oertel, C., Matschullat, J., Zurba, K., Zimmermann, F., Erasmi, S., 2016. Greenhouse gas emissions from soils—A review. Chemie der Erde-Geochemistry 76, 327-352.

Ostertag, R., Hobbie, S.E., 1999. Early stages of root and leaf decomposition in Hawaiian forests: effects of nutrient availability. Oecologia 121, 564-573.

Ott, R.L., Longnecker, M.T., 2015. An introduction to statistical methods and data analysis. Nelson Education.

Parkin, T.B., 1987. Soil microsites as a source of denitrification variability 1. Soil Science Society of America Journal 51, 1194-1199.

Patrick, Z., Toussoun, T., Koch, L., 1964. Effect of crop-residue decomposition products on plant roots. Annual Review of Phytopathology 2, 267-292.

Paustian, K., Six, J., Elliott, E., Hunt, H., 2000. Management options for reducing CO2 emissions from agricultural soils. Biogeochemistry 48, 147-163.

Quigley, M.Y., Rivers, M.L., Kravchenko, A.N., 2018. Patterns and sources of spatial heterogeneity in soil matrix from contrasting long term management practices. Frontiers in Environmental Science 6.

623 Rastogi, M., Singh, S., Pathak, H., 2002. Emission of carbon dioxide from soil. Current
624 Science 82, 510-517.
625 Röver, M., Heinemeyer, O., Munch, J.C., Kaiser, E.-A., 1999. Spatial heterogeneity
626 within the plough layer: high variability of N2O emission rates. Soil Biology and Biochemistry
627 31, 167-173.
628 Roy, J., Mooney, H.A., Saugier, B., 2001. Terrestrial global productivity. pp.83-94.
629 Elsevier.
630 Ruser, R., Flessa, H., Russow, R., Schmidt, G., Buegger, F., Munch, J., 2006. Emission
631 of N2O, N2 and CO2 from soil fertilized with nitrate: effect of compaction, soil moisture and
632 rewetting. Soil Biology and Biochemistry 38, 263-274.
633 SAS Inc., 2017. Base SAS 9.4 procedures guide: Statistical procedures. SAS Institute.
634 Schlüter, S., Zawallich, J., Vogel, H. J., and Dörsch, P.: Physical constraints for
635 respiration in microbial hotspots in soil and their importance for denitrification, Biogeosciences,
636 16, 3665-3678.
637 Schmidt, M.W., Torn, M.S., Abiven, S., Dittmar, T., Guggenberger, G., Janssens, I.A.,
638 Kleber, M., Kögel-Knabner, I., Lehmann, J., Manning, D.A., 2011. Persistence of soil organic
639 matter as an ecosystem property. Nature 478, 49.
640 Schneider, C.A., Rasband, W.S., Eliceiri, K.W., 2012. NIH Image to ImageJ: 25 years of
641 image analysis. Nature methods 9, 671.
642 Sembiring, H., Raun, W., Johnson, G., Boman, R., 1995. Effect of wheat straw inversion
643 on soil water conservation. Soil science 159, 81-89.
644 Shahbaz, M., Kumar, A., Kuzyakov, Y., Börjesson, G., Blagodatskaya, E., 2018.
645 Interactive priming effect of labile carbon and crop residues on SOM depends on residue

646 decomposition stage: Three-source partitioning to evaluate mechanisms. Soil Biology and
647 Biochemistry 126, 179-190.
648 Shelton, D.R., Sadeghi, A.M., McCarty, G.W., 2000. Effect of soil water content on
649 denitrification during cover crop decomposition. Soil science 165(4), pp 365 -371.
650 Sinsabaugh, R., Reynolds, H., Long, T., 2000. Rapid assay for amidohydrolase (urease)
651 activity in environmental samples. Soil Biology and Biochemistry 32, 2095-2097.
652 Strong, D., Wever, H.D., Merckx, R., Recous, S., 2004. Spatial location of carbon
653 decomposition in the soil pore system. European Journal of Soil Science 55, 739-750.
654 Toosi, E., Kravchenko, A., Guber, A., Rivers, M., 2017. Pore characteristics regulate
655 priming and fate of carbon from plant residue. Soil Biology and Biochemistry 113, 219-230.
656 Tufekcioglu, A., Raich, J.W., Isenhart, T.M., Schultz, R.C., 1998. Fine root dynamics,
657 coarse root biomass, root distribution, and soil respiration in a multispecies riparian buffer in
658 Central Iowa, USA. Agroforestry Systems 44, 163-174.
659 van der Weerden, T.J., Kelliher, F.M., de Klein, C.A., 2012. Influence of pore size
660 distribution and soil water content on nitrous oxide emissions. Soil Research 50, 125-135.
661 Vanlauwe, B., Nwoke, O., Sanginga, N., Merckx, R., 1996. Impact of residue quality on
662 the C and N mineralization of leaf and root residues of three agroforestry species. Plant and Soil
663 183, 221-231.
664 Velthof, G.L., Kuikman, P.J., Oenema, O., 2002. Nitrous oxide emission from soils
665 amended with crop residues. Nutrient Cycling in Agroecosystems 62, 249-261.
666 Vessey, J.K., Raper JR, C.D., Henry, L.T., 1990. Cyclic variations in nitrogen uptake rate
667 in soybean plants: uptake during reproductive growth. Journal of experimental botany 41, 1579-
668 1584.

669 Wang, Y., Yu, Z., Li, Y., Wang, G., Liu, J., Liu, J., Liu, X., Jin, J., 2017. Microbial
670 association with the dynamics of particulate organic carbon in response to the amendment of
671 elevated CO2-derived wheat residue into a Mollisol. Science of the Total Environment 607, 972-
672 981.
673 Wildenschild, D., Sheppard, A.P., 2013. X-ray imaging and analysis techniques for
674 quantifying pore-scale structure and processes in subsurface porous medium systems. Advances
675 in Water Resources 51, 217-246.
676 Wildenschild, D., Vaz, C., Rivers, M., Rikard, D., Christensen, B., 2002. Using X-ray
677 computed tomography in hydrology: systems, resolutions, and limitations. Journal of Hydrology
678 267, 285-297.
679

**LIST OF FIGURES**

emission at 75% WFPS, (c) $N_2O$ emission at 50% WFPS, and (d) $N_2O$ emission at 75% WFPS. Shown are the treatment means, the error bars represent standard errors (n=5). Symbols * and ** mark significant differences between pore sizes within the same day ($p < 0.10$ and $p < 0.05$, respectively).

**Fig. 5.** $N_2O$ fluxes during 21-day incubation in large- and small-pore size microcosms at the two studied WFPSs, grouped by pore-size. Shown are the treatment means, the error bars represent standard errors (n=5). Symbol ** marks the differences between WFPSs within the same day ($p < 0.05$).

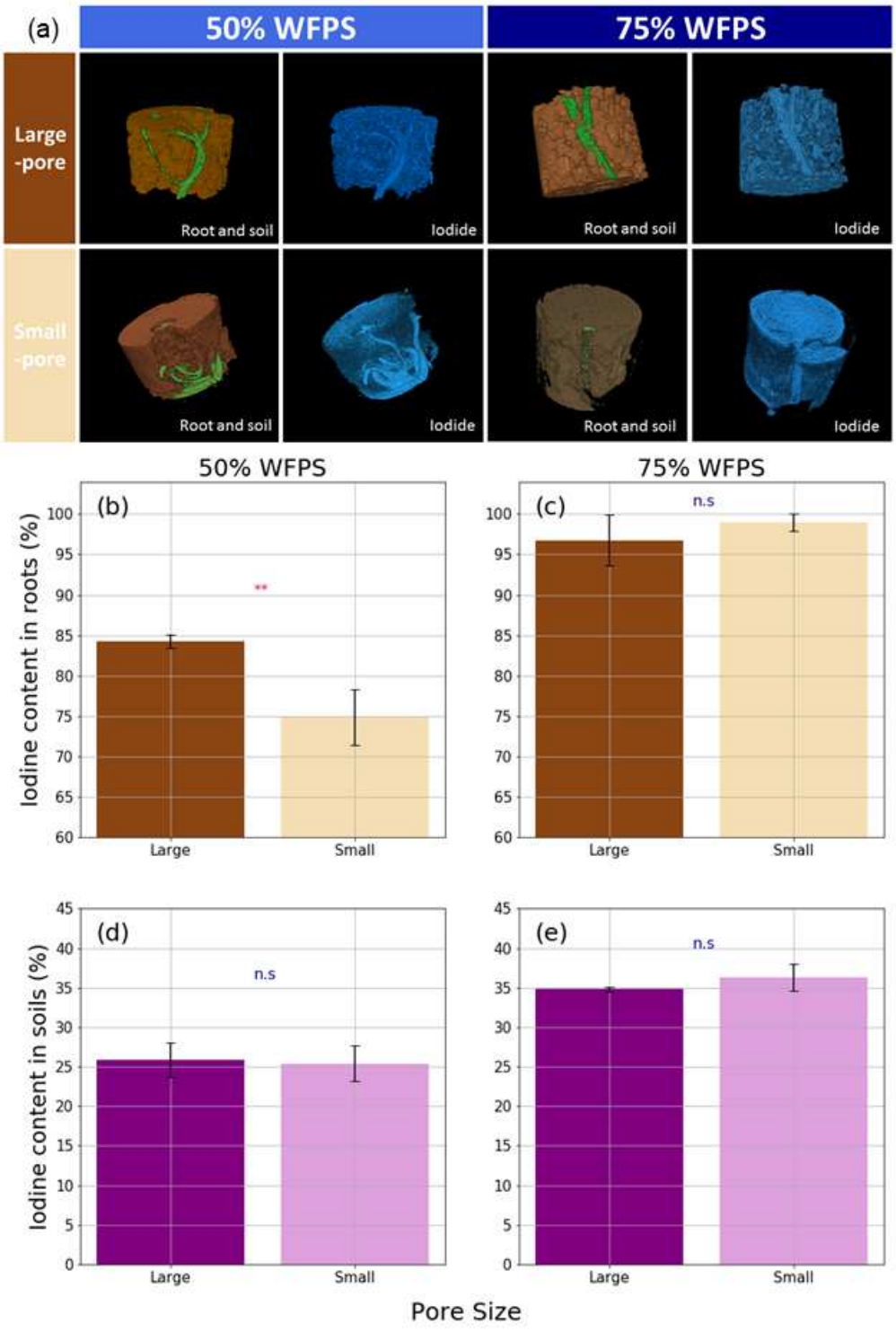
(a)
50% WFPS
75% WFPS
Large -pore
Small -pore
Root and soil
Iodide
50% WFPS
75% WFPS
(b)
(c)
(d)
(e)
**
n.s
Iodine content in roots (%)
Iodine content in soils (%)
Large
Small
Pore Size

**Fig. 1**

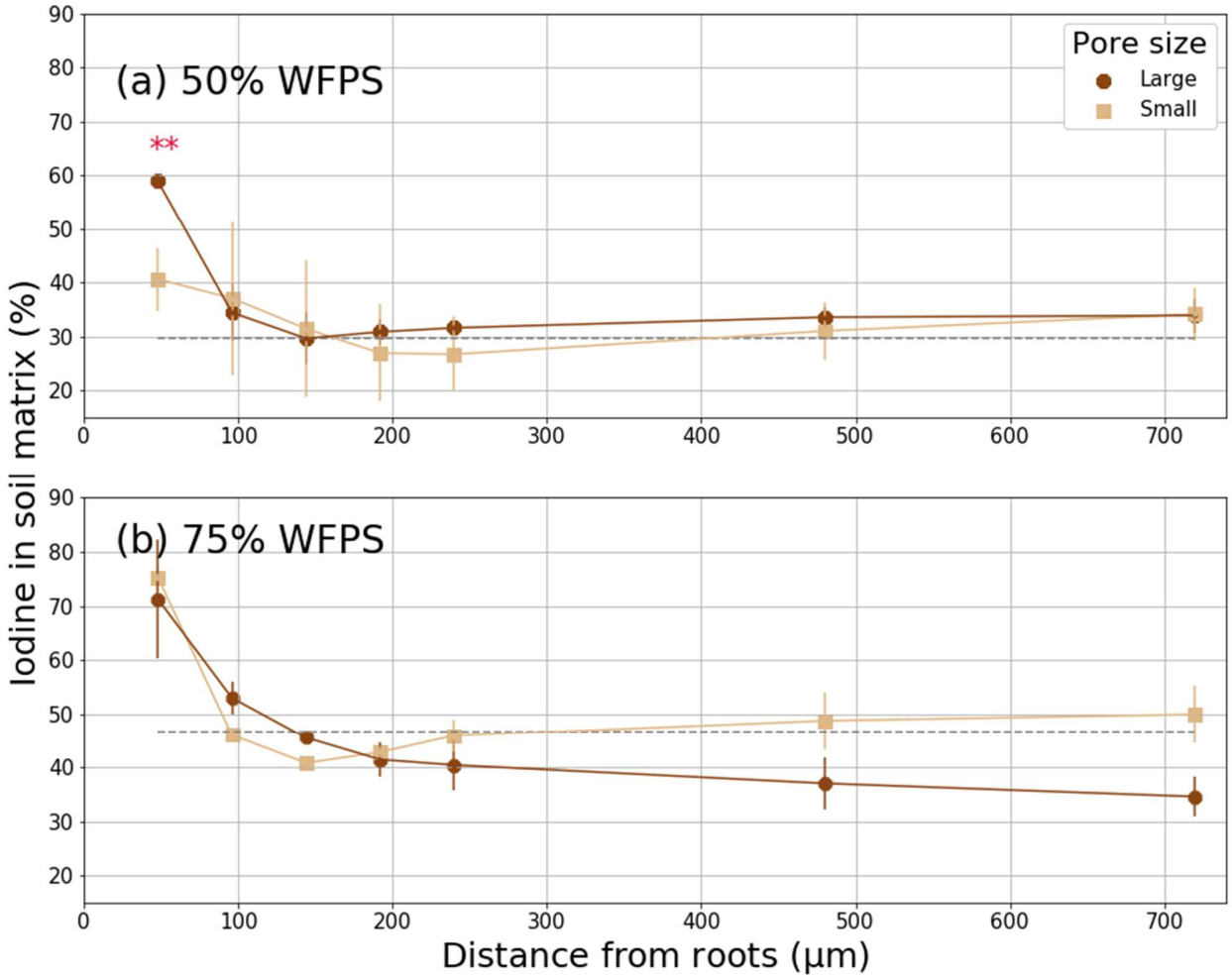
(a) 50% WFPS
**
Pore size
Large
Small
(b) 75% WFPS
Iodine in soil matrix (%)
Distance from roots (µm)

**Fig. 2**

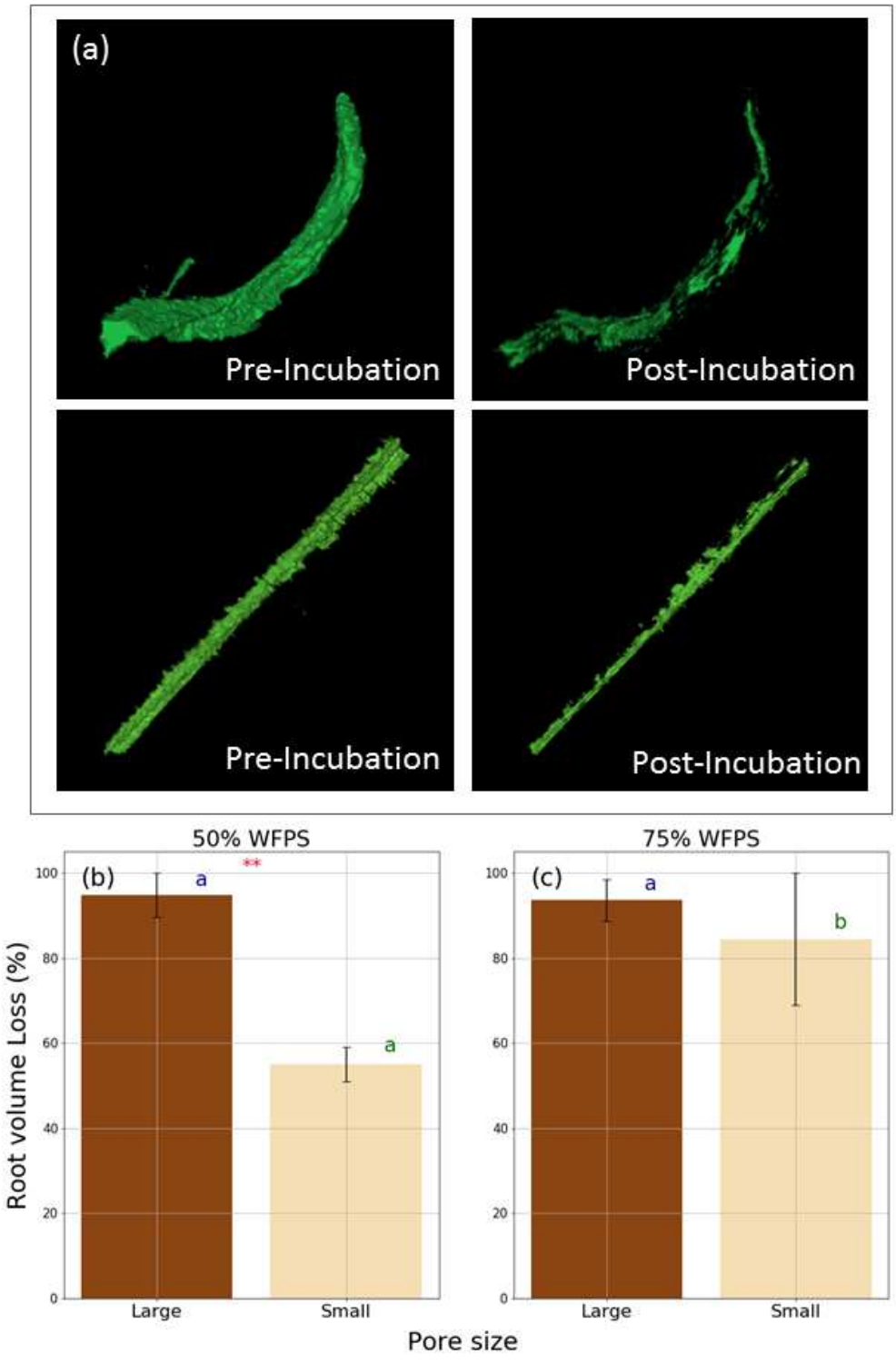
(a)
Pre-Incubation
Post-Incubation
Pre-Incubation
Post-Incubation
50% WFPS
75% WFPS
(b)
(c)
a
**
a
a
b
Root volume Loss (%)
0
20
40
60
80
100
Large
Small
Large
Small
Pore size

**Fig. 3**

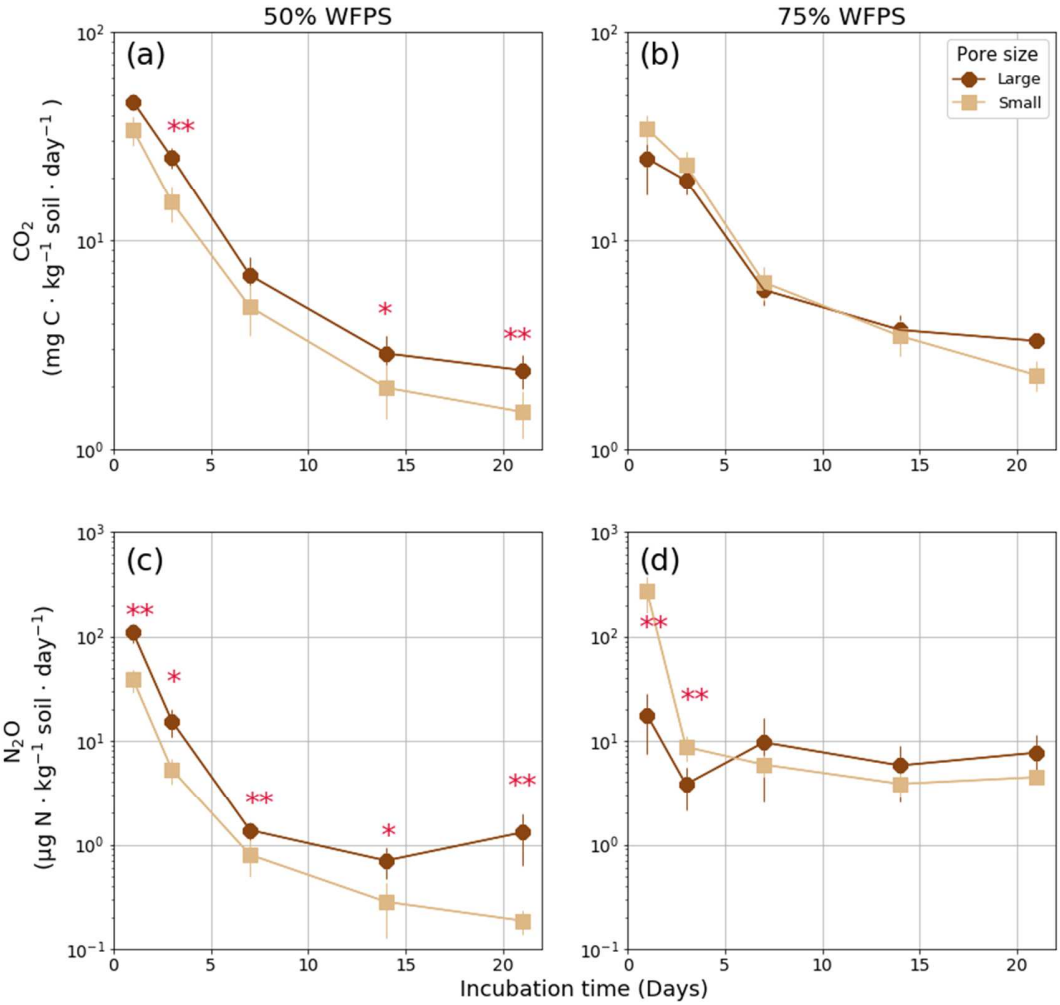
50% WFPS
75% WFPS
(a)
(b)
(c)
(d)
Pore size
Large
Small
$CO_2$ (mg C · kg$^{-1}$ soil · day$^{-1}$)
$N_2O$ (μg N · kg$^{-1}$ soil · day$^{-1}$)
Incubation time (Days)

**Fig. 4**

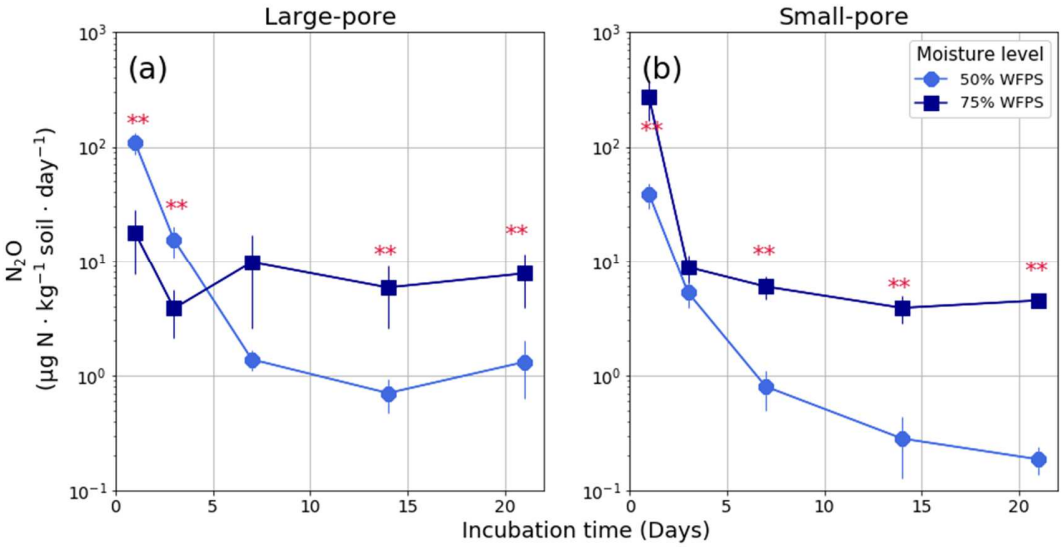
Large-pore
Small-pore
(a)
(b)
Moisture level
50% WFPS
75% WFPS
$N_2O$
(μg N · $kg^{-1}$ soil · $day^{-1}$)
Incubation time (Days)
**

**Fig. 5**

# μCT scanning images

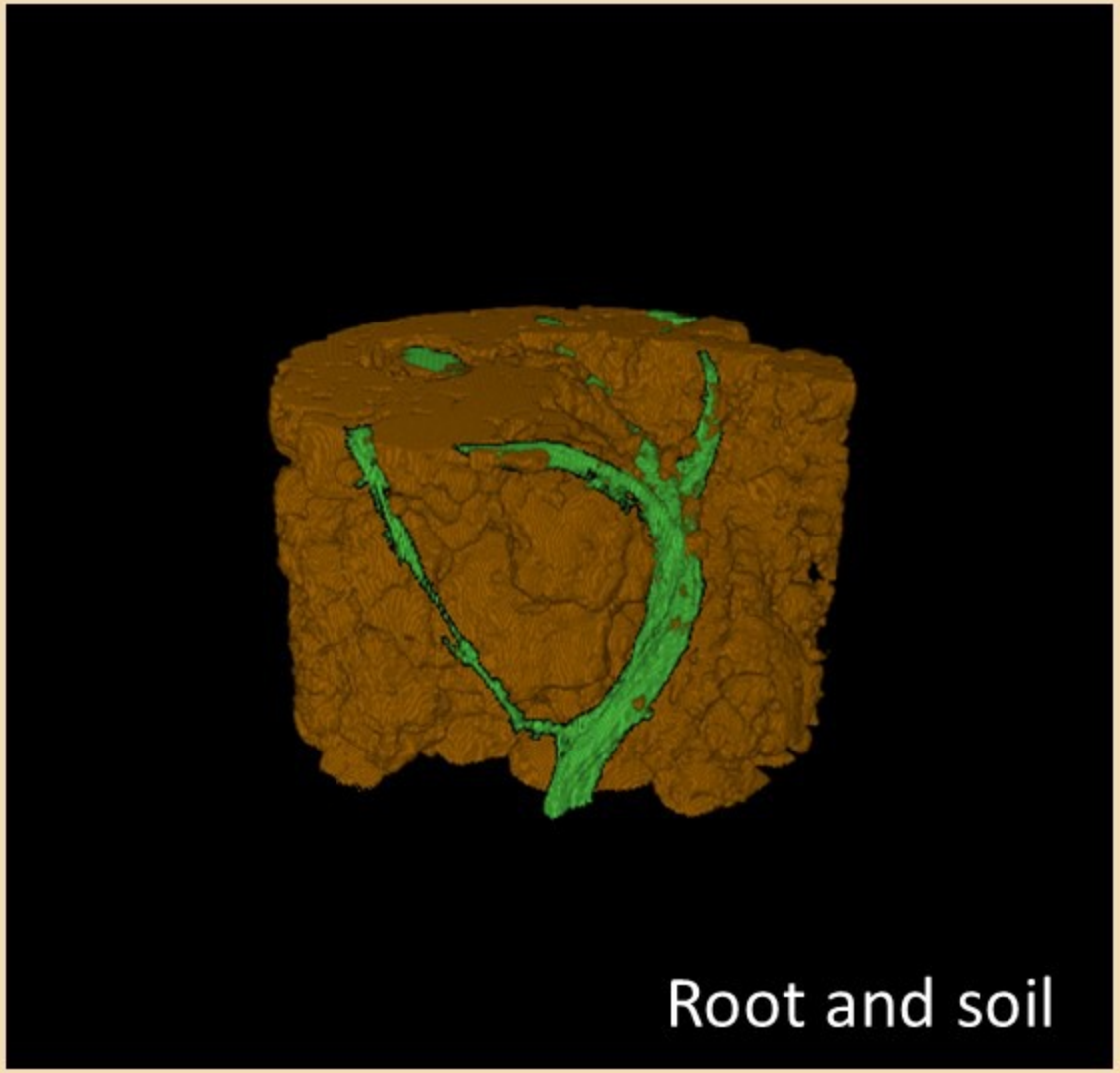

Root and soil

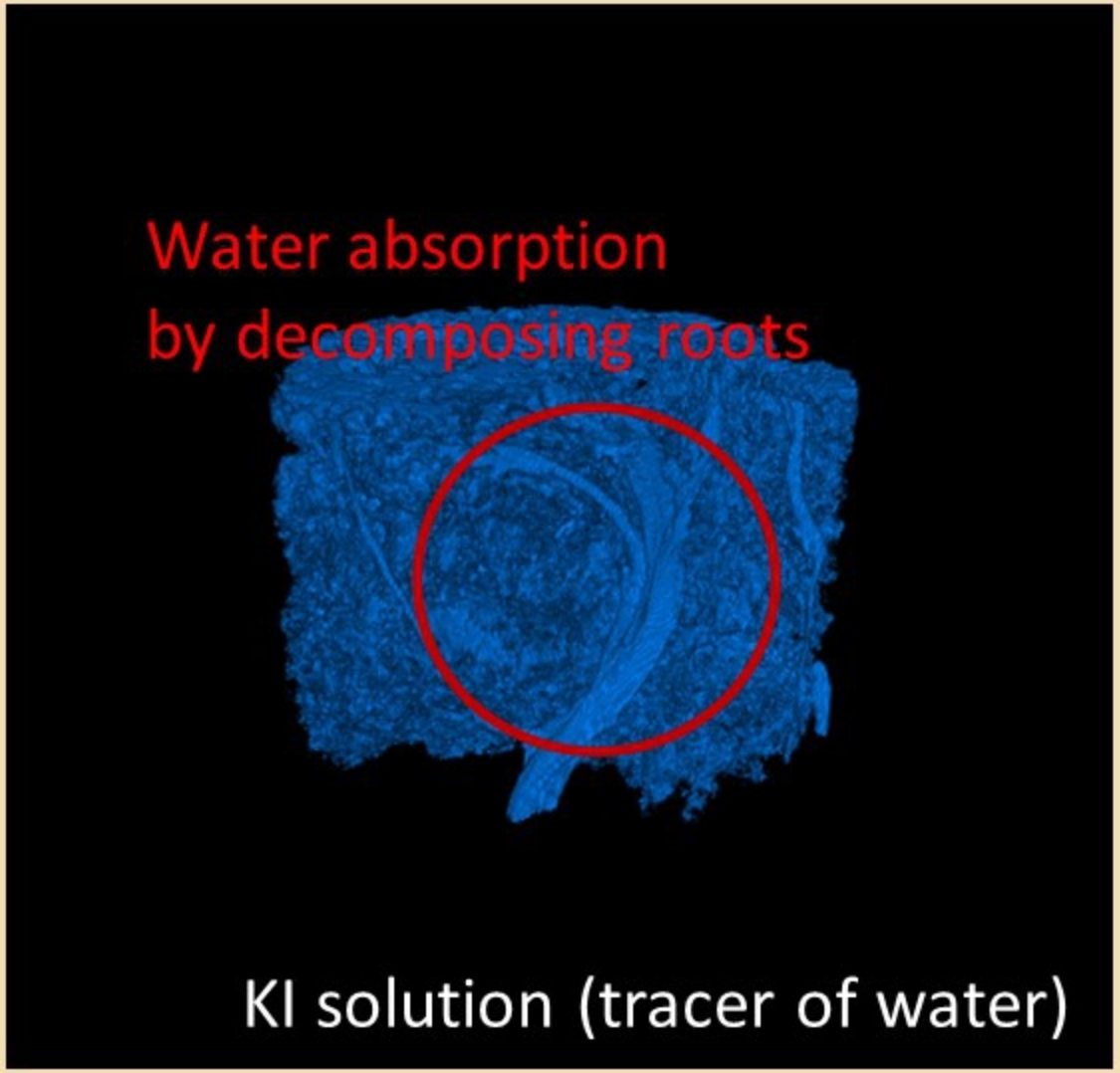


KI solution (tracer of water)